ADVANCED ENERGY MATERIALS
www.advenergymat.de

Water Stable Haloplumbate Modulation for Efficient and Stable Hybrid Perovskite Photovoltaics

*Huanhuan Wang, Zhuang Zhang, Jovana V. Milić, Liguo Tan, Zaiwei Wang, Rong Chen, Xin Jing, Chenyi Yi, Yi Ding, Yuelong Li, Ying Zhao, Xiaodan Zhang, Anders Hagfeldt, Michael Grätzel, and Jingshan Luo**

The commercialization of perovskite solar cells is mainly limited by their operational stability. Interlayer modification by thin interface materials between the perovskite and the charge transport layers is one of the most effective methods to promote the efficiency and stability of perovskite devices. However, the commonly used interlayer materials do not fulfill all the demands, including good film quality, excellent stability, and passivation capability without interfering with the charge transport. In this work, a water stable haloplumbate [TBA]PbI_3 for interfacial modification that meets these demands is proposed, which is formed on the perovskite surface in situ by *tetra*-butylammonium iodide treatment. Benefiting from its passivation effect and robustness, the modified devices result in a power conversion efficiency of 22.90% with enhanced environmental and operational stability. In addition, the self-limiting effect of the reaction contributes to the controllability of device fabrication and the repeatability of device performance.

1. Introduction

Perovskite solar cells (PSCs) have shown great promise for photovoltaic applications due to their low cost and high power conversion efficiency (PCE).[1–7] Their PCE has increased from 3.8%[8] to certified 25.5%[9] in the past decade, ascribed to their excellent optical and electronic properties, such as tunable bandgap, high absorption coefficient, and long charge carrier lifetime.[2,10–12] However, the instability of perovskite materials still restricts their large-scale commercialization.[1,13–15] This is the result of multiple factors, such as the reactivity to moisture, oxygen, thermal stress, voltage bias, and light, which cause the unexpected degradation of PSCs.[16–18]

In recent years, among all the methods for improving the stability of PSCs,[19,20] interfacial engineering of thin interlayers on the surface of the perovskite layer is proved to be one of the most effective methods.[21,22] This has involved various molecular assemblies[23–26] as well as graphene composites,[27] along with low-dimensional perovskites,[28,29] polymers,[30] and inorganic materials.[31] An ideal interfacial modulator should fulfill several requirements, namely: (i) forming a well-defined compact structure with good coverage, (ii) featuring excellent stability against environmental and operational conditions, with (iii) appropriate energy alignment, along with the (iv) passivation capacity. A compact and well-covered interlayer can prevent water and oxygen from damaging the perovskite layer underneath, while preventing the volatile species from being released, whereas the interlayer itself should be stable against moisture, oxygen, thermal, and other operating factors to provide long-term protection. Finally, the interlayer should ideally have a good energy level alignment, so that it would not limit the charge carrier transport, while it should also be able to passivate defects on the surface of the perovskite

H. Wang, Z. Zhang, Dr. R. Chen, X. Jing, Prof. Y. Ding, Prof. Y. Li, Prof. Y. Zhao, Prof. X. Zhang, Prof. J. Luo
Institute of Photoelectronic Thin Film Devices and Technology
Key Laboratory of Photoelectronic Thin Film Devices and Technology of Tianjin
Ministry of Education Engineering Research Center of Thin Film Photoelectronic Technology
Renewable Energy Conversion and Storage Center
Nankai University
Tianjin 300350, China
E-mail: jingshan.luo@nankai.edu.cn

Dr. J. V. Milić, Prof. M. Grätzel
Laboratory of Photonics and Interfaces
Institute of Chemical Sciences and Engineering
Ecole Polytechnique Fedérale de Lausanne (EPFL)
Lausanne 1015, Switzerland

Dr. J. V. Milić
Adolphe Merkle Institute
University of Fribourg
Fribourg 1700, Switzerland

L. Tan, Prof. C. Yi
State Key Laboratory of Power System
Department of Electrical Engineering
Tsinghua University
Beijing, China

Dr. Z. Wang, Prof. A. Hagfeldt
Laboratory of Photomolecular Science
Institute of Chemical Sciences Engineering
Ecole Polytechnique Fedérale de Lausanne (EPFL)
Lausanne 1015, Switzerland

The ORCID identification number(s) for the author(s) of this article can be found under https://doi.org/10.1002/aenm.202101082.

DOI: 10.1002/aenm.202101082

layer, which could contribute to the overall photovoltaic performance.

Haloplumbates are low-dimensional organolead halide complexes which contain a lead halide [Pb_nX_m] octahedral framework different from the one in hybrid halide perovskites. They have been studied due to their diverse crystal structure,[32–36] luminescence,[36–39] and thermal stability.[32,34,40] Recently, $[Pb_8I_8(H_2O)_3]^{8+}[^-O_2C(CH_2)_4CO_2^-]_4$ haloplumbate was used for photocatalytic water splitting, showing excellent photoelectrical properties and superior moisture resistance.[41] *Tetra*-butylammonium lead iodide ([TBA]PbI_3) is another type haloplumbate with excellent stability in water and under thermal stress.[31,42] Based on these unique properties, haloplumbates are potential candidates for interfacial modulators of hybrid perovskite devices.

TBA^+ has been reported to assist crystallization and film formation to improve photovoltaic performance and act as hydrophobic materials to promote stability with formation of low-dimensional materials when used as additives,[43–47] and most recently, as post-treatment materials[48,49] during the submission of this paper. Inspired by these results, it is possible to form [TBA]PbI_3 haloplumbate on the surface of perovskite with TBAI treatment. In this work, we systematically studied the properties of [TBA]PbI_3 and introduced it on the surface of the perovskite layer through an in situ reaction between the perovskite and TBAI, which was found to be self-limiting and well-defined on the surface of perovskite layer without affecting the underlayer while significantly reducing the trap density. As a result, we obtained solar cells with efficiencies up to 22.90% and enhanced stability against moisture and heat under operating conditions.

2. Results and Discussion

The haloplumbate single crystal of [TBA]PbI_3 was isolated through slow evaporation process of the precursor solution of PbI_2 and TBAI (**Figure 1**a; experimental details provided in

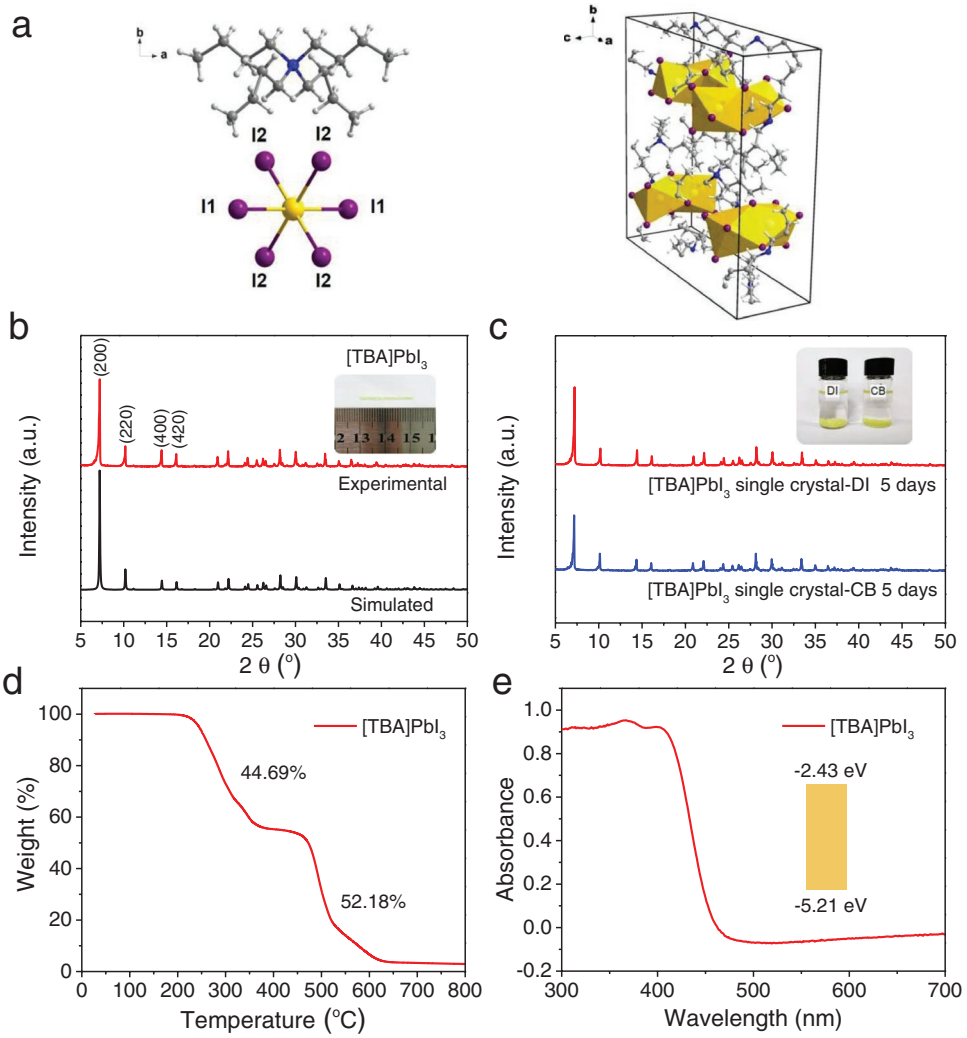

Figure 1. Characterization of [TBA]PbI_3 haloplumbate phase. a) Simulated and experimental X-ray diffraction (XRD) patterns of [TBA]PbI_3 single crystals. The simulated pattern is based on the reported structure of [TBA]PbI_3 (CCDC no. 994586).[42] b) Crystal structure of [TBA]PbI_3. c) XRD patterns of [TBA]PbI_3 single crystals immersed into deionized water (DI) and chlorobenzene (CB) for 5 days. d) Thermogravimetric analysis of [TBA]PbI_3 single crystals. e) UV–vis absorption spectrum of [TBA]PbI_3. The inset shows the energy band gap of [TBA]PbI_3 and the valence and conduction band positions.

the supporting information), forming yellow rod-like crystals (Figure S1, Supporting Information). The X-ray diffraction (XRD) pattern of the crystal is identical with the calculated [TBA]PbI_3 pattern (Figure 1b), evidencing its formation. It crystallizes in tetragonal space group *I*-42d with a 1D face-sharing inorganic chain (Figure 1a).

To assess the stability to moisture, the [TBA]PbI_3 crystals were immersed into deionized (DI) water at ambient temperature. Moreover, since chlorobenzene (CB) is used for depositing the charge transport layer, the stability in CB was also tested. The XRD patterns of [TBA]PbI_3 crystals in DI water and CB show no apparent change after 5 days (Figure 1c), suggesting that [TBA]PbI_3 is stable under these conditions. The thermal stability was further tested by thermogravimetric analysis (TGA) to show that [TBA]PbI_3 remains stable below 200 °C (Figure 1d), losing 44.69% weight only at 210–380 °C and the remaining 52.18% weight at 380–640 °C, which corresponds to the volatilization of TBAI and the sublimation of lead iodide (PbI_2), respectively.[42] The TGA demonstrates excellent stability of [TBA]PbI_3 against heat in the typical temperature range of perovskite device operation. Finally, the energy band structure of [TBA]PbI_3 was analyzed by the UV-Vis diffuse reflection (Figure S2a,b, Supporting Information) and the valence band X-ray photoelectron spectroscopy (VBXPS; Figure S3, Supporting Information). The valence band maximum (VBM) of [TBA]PbI_3 was found to be 5.21 eV (Figure 1e; procedure described in the supporting information), between the VBM of widely used hybrid perovskite compositions and the highest occupied molecular orbital (HOMO) of 2,2′,7,7′-tetrakis[*N*,*N*-di(4-methoxyphenyl)amino]-9,9′-spirobifluorene (Spiro-OMeTAD; Figure S4, Supporting Information), which is beneficial for the hole transport.[50,51] In summary, [TBA]PbI_3 has shown excellent water and thermal stability, as well as good energy band alignment, suggesting that it can be a suitable interfacial modulator.

Having demonstrated these excellent properties of [TBA]PbI_3, it was deposited onto the perovskite surface by using the solution of TBAI in chloroform ($CHCl_3$), a solvent that was shown not to affect the perovskite layer.[52] This procedure results in the formation of the [TBA]PbI_3 in situ (experimental details are provided in the Experimental Section). The mixed organic cation perovskite $FA_{1-x}MA_xPbI_3$ was deposited by a two-step spin-coating method as control sample.[25,53] The [TBA]PbI_3 layer is envisaged to exist on the surface of the perovskite layer without damaging the perovskite grains (**Figure 2**a). The top-view scanning electron microscopy (SEM) images (Figure 2b,c) show an obvious change of perovskite film morphology after the treatment, which involves reducing the number of pinholes and grain boundaries that may cause shunts and stronger non-radiative recombination. Upon TBAI treatment, a thin layer with good coverage forms on the surface of the perovskite layer, which fills the pinholes and grain boundaries. This is in accordance with the atomic force microscopy (AFM) (Figure S5a,b, Supporting Information) showing a reduced Root Mean Square roughness from 33.5 to 21.3 nm. To assess the structural properties of the layer, XRD measurements were performed. The XRD patterns (Figure 2d) show four new diffraction peaks at 7.2°, 10.2°, 14.44°, and 16.16°, corresponding to the ⟨200⟩, ⟨220⟩, ⟨400⟩, and ⟨420⟩ planes of [TBA]PbI_3, respectively.[42] Furthermore, the intensity of the PbI_2 peak at 12.6° decreases after TBAI treatment upon formation of [TBA]PbI_3 comes through the reaction with PbI_2. This is further evidenced by the XRD patterns of the PbI_2 films treated with TBAI (Figure S6,

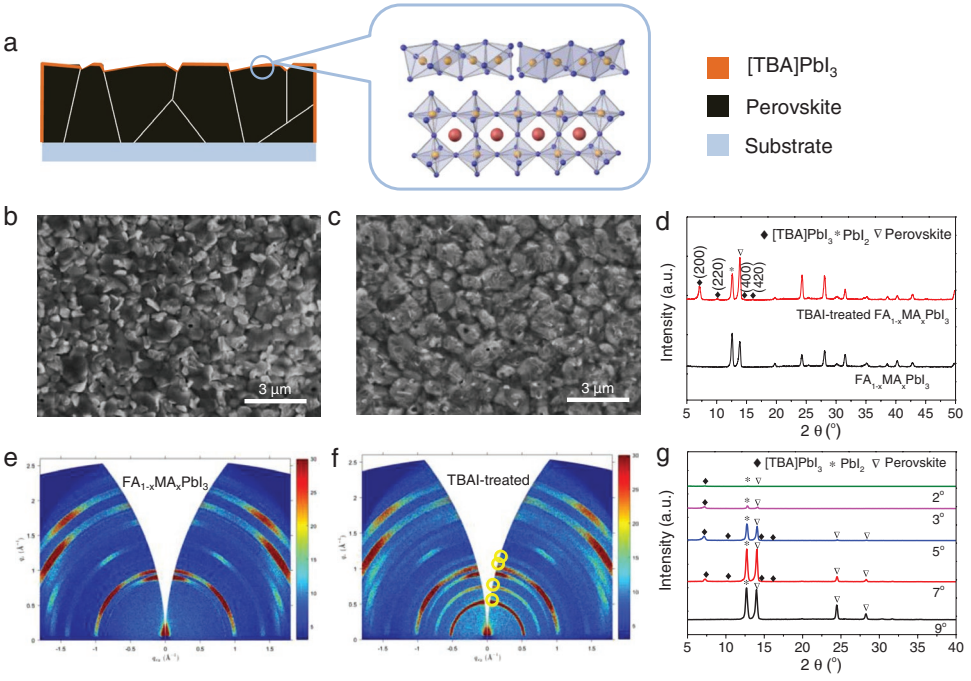

Figure 2. Modulated perovskite film characterization. a) Simplified scheme presenting the perovskite films modulated with [TBA]PbI_3. b–c) Top-view scanning electron microscopy (SEM) images of the $FA_{1-x}MA_xPbI_3$ and TBAI-treated perovskite films. d) XRD patterns of the $FA_{1-x}MA_xPbI_3$ and TBAI-treated perovskite films. e,f) Two-dimensional (2D) grazing-incidence X-ray diffraction (GIXRD) patterns of $FA_{1-x}MA_xPbI_3$ and TBAI-treated perovskite films (yellow circles in f indicate the formation of new signals). g) GIXRD patterns of TBAI-treated perovskite films at different incidence angles.

Supporting Information), which revealed the formation of [TBA]PbI_3 under these conditions. 2D grazing-incidence X-ray diffraction (GIXRD) patterns (Figure 2e,f) show four new scattering rings upon TBAI treatment, evidencing formation of 1D [TBA]PbI_3 on the surface of perovskite layer in random directions parallel to the substrate. After TBAI treatment, the film still maintained proper band alignment, as illustrated by the band energy diagram derived from the VBXPS and UV–vis spectra (Figure S7, Supporting Information).

Interestingly, the reaction between the perovskite and TBAI was found to be self-limiting. In general, when depositing a 2D perovskite overlayer through an in situ reaction process, the larger organic cations exchange with the smaller cations in the perovskite layer continuously until the entire 3D perovskite layer is converted to 2D perovskite.[54] In contrast, the reaction between perovskite and TBAI stops after forming a thin layer of [TBA]PbI_3. To demonstrate this, we immersed three perovskite films into isopropanol (IPA) and the solutions of either *n*-butylammonium iodide (BAI) or TBAI in IPA (Figure S8, Supporting Information). The BAI was employed as a widely used organic cation for 2D perovskites. The edge of the film in IPA turns yellow after 6 hours as the perovskite layer suffers from degradation in IPA, whereas the film immersed in the solution of BAI completely turns yellow after the same period of time. The XRD patterns of the corresponding films (Figure S9a, Supporting Information) show intense PbI_2 peaks and weaker perovskite peaks over time, indicating that the cation exchange process accelerates the degradation of the film. However, the film placed in the TBAI solution remains black even after 24 h, and the corresponding XRD patterns maintain the original intensity (Figure S9b, Supporting Information), indicating that the reaction is self-limiting.

As a result, the TBAI treatment is supposed to influence the surface of the perovskite without affecting the bulk. To probe this effect on the distribution of [TBA]PbI_3, we analyzed GIXRD with different incidence angles (Figure 2g). With the increase of the incidence angles, the perovskite peak intensities increase, yet the [TBA]PbI_3 peaks become stronger for incidence angles up to 5°, after which they become weaker and disappear with further increase of the angle of incidence. This suggests that [TBA]PbI_3 mainly exists on the surface of the perovskite layer,[55,56] which is further analyzed by X-ray photoelectron spectroscopy (XPS). The XPS spectra of perovskite films show shifts of peak positions in the N 1s core level range (Figure S10a, Supporting Information), featuring two peaks at binding energies of 400.15 and 400.45 eV, corresponding to the N atoms in the formamidinium (FA^+) A cation.[57] In the [TBA]PbI_3-modulated sample, there is only one peak at 401.38 eV corresponding to $N(C_4H_9)_4^+$, which indicates complete transformation of the perovskite to [TBA]PbI_3 on the surface. The Pb 4f and C 1s core level spectra (Figure S10b,c, Supporting Information) also show apparent peak shifts upon [TBA]PbI_3 modulation. In addition, the C=O signal at 288.05 eV in the C1s spectra (Figure S10c, Supporting Information) of the control sample disappears upon TBAI treatment, which suggests that $TBAPbI_3$ could protect perovskite from moisture and oxygen in the air.[25] To prove this effect, we immersed the perovskite films into DI water (Movies S1 and S2, Supporting Information). While the control film completely turns yellow after 7 s, the [TBA]PbI_3-modulated film (obtained by immersing the perovskite film into TBAI solution) remains black in 1 min, indicating that the [TBA]PbI_3 interlayer have an obvious protective effect against water.

We thereafter investigated optical and electronic properties of the [TBA]PbI_3-modulated films and devices. The steady state photoluminescence (PL) spectroscopy (**Figure 3**a) shows a fivefold enhancement in PL intensity upon TBAI treatment, suggesting that [TBA]PbI_3 might passivate the defects of perovskite film to suppress the non-radiative recombination. Accordingly, time-resolved photoluminescence (TRPL) spectroscopy (Figure 3b) reveals an increase in charge carrier lifetimes from 500.01 to 1049.03 ns (Table S1, Supporting Information), whereas confocal PL mapping of control and [TBA]PbI_3-modulated perovskite films (Figure 3c,d) shows an increase in the PL brightness of the surface from 120.60 to 155.26 after TBAI treatment. This is likely caused by the passivation of defects on the surface and at the grain boundaries of the perovskite.[58] To quantify the electron-trap densities (n_t) in the control and [TBA]PbI_3-modulated devices, the space-charge-limited-current (SCLC) measurements were performed (experimental details are provided in the Experimental Section) with an electron-only device structure of ITO/SnO_2/$FA_{1-x}MA_xPbI_3$/PCBM/Au (ITO for indium tin oxide; Figure S11, Supporting Information).[53,59] The trap filled limit voltage (V_{TFL}) decreases from 1.050 to 0.625 V, corresponding to the reduced density of trap states in the perovskite film from 9.9×10^{15} to 5.9×10^{15} cm^{-3} upon TBAI treatment, which is particularly relevant for the photovoltaic performances.[50,53]

The photovoltaic devices were fabricated with the ITO/SnO_2/$FA_{1-x}MA_xPbI_3$/spiro-OMeTAD/Au architecture as our previous report, as shown in the cross-sectional SEM image (Figure S12, Supporting Information).[53] The best device demonstrated the efficiency of 22.90% (V_{OC} = 1.15 V, J_{SC} = 24.81 mA cm^{-2}, FF = 80.27%), which has been improved as compared to the control device with an efficiency of 21.53% (V_{OC} = 1.12 V, J_{SC} = 24.80 mA cm^{-2}, FF = 77.64%, **Figure 4**a). In addition, the [TBA]PbI_3-modulated device showed a lower hysteresis factor compared to control device (Figure S13 and Table S2, Supporting Information). The average efficiency and repeatability were also improved (Figure S14, Supporting Information), whereas the integrated current density calculated from the external quantum efficiency (EQE) was found to be 23.94 mA cm^{-2} (Figure 4b), which is consistent with the current–voltage (*J*–V) measurements. This improvement in the photovoltaic performances is likely related to the passivation effect of [TBA]PbI_3.

To further study the dynamics of carriers, we analyzed the transient photovoltage decay (TPV). TPV decay curves (Figure 4c) show a higher recombination time constant (τ_r), from 2.87 to 6.45 µs, which could be attributed to the slower surface recombination in the modulated device.[25] Electrical impedance spectroscopy (EIS) spectra (Figure S15, Supporting Information) also corroborated with the reduced non-radiative recombination, showing increased recombination resistance (R_{re}) of the [TBA]PbI_3-modulated device from 2736 to 3646 Ω (Table S3, Supporting Information).[60,61]

Considering the self-limiting feature of the [TBA]PbI_3 layer, devices with the perovskite layer immersed in the TBAI

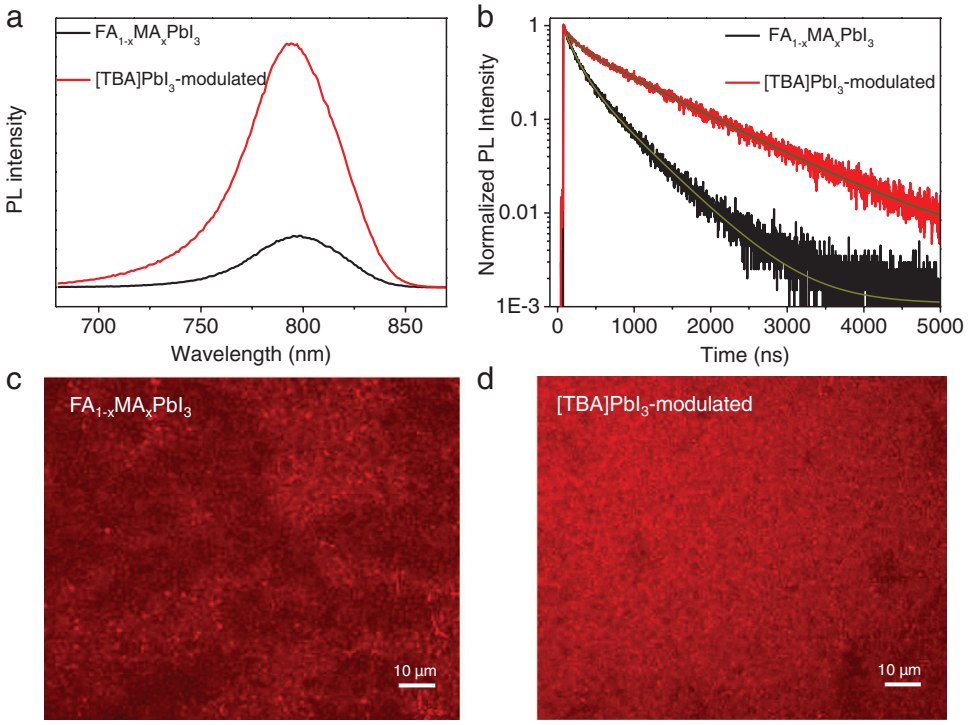

Figure 3. Photoluminescence of modulated perovskite films. a) Steady state PL spectra of $FA_{1-x}MA_xPbI_3$ and $[TBA]PbI_3$-modulated perovskite films. b) Time-resolved photoluminescence spectra of $FA_{1-x}MA_xPbI_3$ and $[TBA]PbI_3$-modulated perovskite films. c,d) Confocal PL mapping of the intensity on $FA_{1-x}MA_xPbI_3$ and $[TBA]PbI_3$-modulated perovskite films.

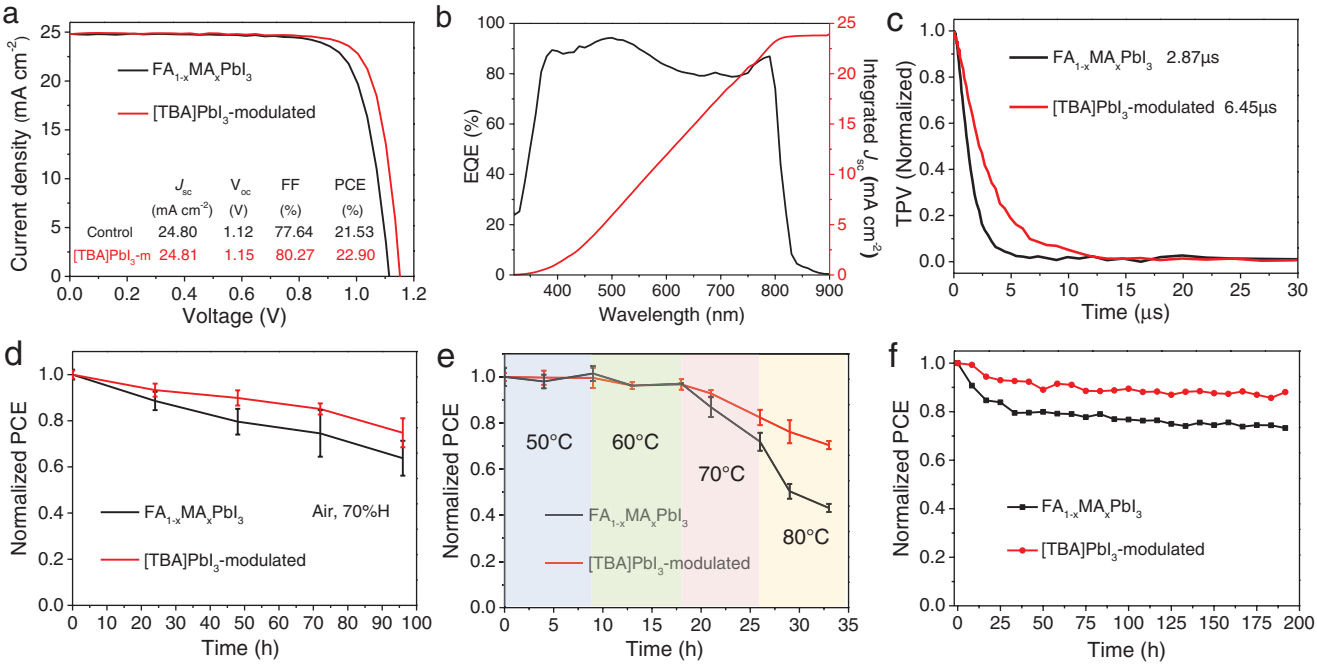

Figure 4. Device performance and stability. a) Current density–voltage (*J–V*) curves of $FA_{1-x}MA_xPbI_3$ and $[TBA]PbI_3$-modulated devices. b) External quantum efficiency (EQE) spectra of $[TBA]PbI_3$-modulated device. c) Normalized transient photovoltage (TPV) decay curves of $FA_{1-x}MA_xPbI_3$ and $[TBA]PbI_3$-modulated devices. d) Normalized power conversion efficiency (PCE) of devices stored in the air with 70% relatively humidity (RH) under dark. e) Normalized PCE of devices stored in nitrogen-filled glove box under elevated temperatures, five control devices and five $[TBA]PbI_3$-modulated devices were tested, the error bars were based on results of five devices, and they are the standard deviations. f) Normalized PCE of devices measured by maximum power point tracking (MPPT) under 1 sun illumination at room temperature.

solution in $CHCl_3$ for different periods of time show almost identical *J–V* curves, evidencing that the immersion time does not influence the device performance (Figure S16 and Table S4, Supporting Information). To exclude the effect of the solvent used, we compared the performances of the control devices, the $CHCl_3$ modulated devices, and the TBAI/$CHCl_3$ solution treated ones (Figure S17, Supporting Information). The results show that the $CHCl_3$ modulated devices have no increase in efficiency and repeatability.

We thereby investigated the humidity, thermal, operational, and long-term stability of [TBA]PbI_3-modulated devices. We exposed the control and [TBA]PbI_3-modulated perovskite films to air at 75% relative humidity (RH) at ambient temperature and monitored their changes. While the control film decomposed after 48 h, the [TBA]PbI_3-modulated film featured no visual change after 120 h (Figure S18, Supporting Information). Accordingly, the efficiencies of [TBA]PbI_3-modulated devices show higher resilience than the control devices in the moist air (Figure 4d). The thermal stability of the [TBA]PbI_3-modulated devices is also improved, especially at temperatures above 70 °C (Figure 4e). The [TBA]PbI_3-modulated perovskite films show a lower decomposition rate (Figure S19, Supporting Information) under environmental conditions and thermal stress. In addition, the efficiencies of devices show no change under long-term storage (Figure S20, Supporting Information). Under continuous maximum power point tracking operation, the [TBA]PbI_3-modulated device maintains 86% efficiency after 200 h while the efficiency of the control device reduced significantly (Figure 4f).

3. Conclusion

In summary, we have introduced water stable haloplumbate materials based on *tetra*-butylammonium (TBA) organic moieties as the interfacial modulator for PSCs. The self-limiting haloplumbate [TBA]PbI_3 layer forms in situ at the interface between perovskite and hole transport layer with enhanced stability and matched band energy level alignment. The modulated perovskite samples show reduced trap density and increased water stability. As a result, the champion photovoltaic device has a power conversion efficiency of 22.90%, along with enhanced stability under environmental and operational conditions, as well as long-term storage. The remarkable stability and the favorable effects on perovskite materials as well as the ease of fabrication render haloplumbate-based interfacial modulators ideal candidates for addressing the stability problem that impedes the commercialization of PSCs.

Supporting Information

Supporting Information is available from the Wiley Online Library or from the author.

Acknowledgements

H.W. and Z.Z. contributed equally to this work. The authors would like to thank Dr. Ke Meng for the GIXRD characterization. This study was supported by the National Key Research and Development Program of China (Grant No. 2018YFB1502003, 2019YFE0123400), the Tianjin Distinguished Young Scholars Fund (20JCJQJC00260), the Chinese Thousand Talents Program for Young Professionals, the "111" Project (Grant No. B16027), National Natural Science Foundation of China (Grant No. 21872080), and the startup funding of Nankai University. J.V.M. is grateful for the Swiss National Science Foundation no. 193174.

Conflict of Interest

The authors declare no conflict of interest.

Data Availability Statement

Research data are not shared.

Keywords

interlayer modification, perovskite solar cells, water stable haloplumbates

Received: April 5, 2021
Revised: April 30, 2021
Published online:

[1] Y. Rong, Y. Hu, A. Mei, H. Tan, M. I. Saidaminov, S. I. Seok, M. D. McGehee, E. H. Sargent, H. Han, *Science* **2018**, 361.
[2] A. K. Jena, A. Kulkarni, T. Miyasaka, *Chem. Rev.* **2019**, *119*, 3036.
[3] S. H. Turren-Cruz, A. Hagfeldt, M. Saliba, *Science* **2018**, *362*, 449.
[4] E. H. Jung, N. J. Jeon, E. Y. Park, C. S. Moon, T. J. Shin, T. Y. Yang, J. H. Noh, J. Seo, *Nature* **2019**, *567*, 511.
[5] W. Nie, H. Tsai, R. Asadpour, J. C. Blancon, A. J. Neukirch, G. Gupta, J. J. Crochet, M. Chhowalla, S. Tretiak, M. A. Alam, H. L. Wang, A. D. Mohite, *Science* **2015**, *347*, 522.
[6] G. Kim, H. Min, K. S. Lee, D. Y. Lee, S. M. Yoon, S. I. Seok, *Science* **2020**, *370*, 108.
[7] H. Lu, Y. Liu, P. Ahlawat, A. Mishra, W. R. Tress, F. T. Eickemeyer, Y. Yang, F. Fu, Z. Wang, C. E. Avalos, B. I. Carlsen, A. Agarwalla, X. Zhang, X. Li, Y. Zhan, S. M. Zakeeruddin, L. Emsley, U. Rothlisberger, L. Zheng, A. Hagfeldt, M. Gratzel, *Science* **2020**, *370*, 74.
[8] A. Kojima, K. Teshima, Y. Shirai, T. Miyasaka, *J. Am. Chem. Soc.* **2009**, *131*, 6050.
[9] Best Research-Cell Efficiencies (NREL, 2021); https://www.nrel.gov/pv/cell-efficiency.html
[10] S. D. Stranks, G. E. Eperon, G. Grancini, C. Menelaou, M. J. Alcocer, T. Leijtens, L. M. Herz, A. Petrozza, H. J. Snaith, *Science* **2013**, *342*, 341.
[11] Q. Dong, Y. Fang, Y. Shao, P. Mulligan, J. Qiu, L. Cao, J. Huang, *Science* **2015**, *347*, 967.
[12] K. Lin, J. Xing, L. N. Quan, F. P. G. de Arquer, X. Gong, J. Lu, L. Xie, W. Zhao, D. Zhang, C. Yan, W. Li, X. Liu, Y. Lu, J. Kirman, E. H. Sargent, Q. Xiong, Z. Wei, *Nature* **2018**, *562*, 245.
[13] M. Gratzel, *Nat. Mater.* **2014**, *13*, 838.
[14] S. Yang, Y. Wang, P. Liu, Y.-B. Cheng, H. J. Zhao, H. G. Yang, *Nat. Energy* **2016**, *1*, 15016.
[15] T. Leijtens, G. E. Eperon, N. K. Noel, S. N. Habisreutinger, A. Petrozza, H. J. Snaith, *Adv. Energy Mater.* **2015**, *5*, 1500963.
[16] R. Wang, M. Mujahid, Y. Duan, Z. K. Wang, J. Xue, Y. Yang, *Adv. Funct. Mater.* **2019**, *29*, 1808843.

[17] E. T. Hoke, D. J. Slotcavage, E. R. Dohner, A. R. Bowring, H. I. Karunadasa, M. D. McGehee, *Chem. Sci.* **2015**, *6*, 613.
[18] J. Wei, Q. Wang, J. Huo, F. Gao, Z. Gan, Q. Zhao, H. Li, *Adv. Energy Mater.* **2021**, *11*, 2002326.
[19] F. Zhang, K. Zhu, *Adv. Energy Mater.* **2020**, *10*, 1902579.
[20] F. Zhang, C. Xiao, X. Chen, B. W. Larson, S. P. Harvey, J. J. Berry, K. Zhu, *Joule* **2019**, *3*, 1452.
[21] S. Shao, M. A. Loi, *Adv. Mater. Interfaces* **2019**, *7*, 1901469.
[22] F. Zhang, H. Lu, B. W. Larson, C. Xiao, S. P. Dunfield, O. G. Reid, X. Chen, M. Yang, J. J. Berry, M. C. Beard, K. Zhu, *Chem* **2021**, *7*, 774.
[23] J. V. Milic, D. J. Kubicki, L. Emsley, M. Gratzel, *Chimia (Aarau)* **2019**, *73*, 317.
[24] H. Zhang, M. K. Nazeeruddin, W. C. H. Choy, *Adv. Mater.* **2019**, *31*, 1805702.
[25] Q. Jiang, Y. Zhao, X. Zhang, X. Yang, Y. Chen, Z. Chu, Q. Ye, X. Li, Z. Yin, J. You, *Nat. Photonics* **2019**, *13*, 460.
[26] R. Wang, J. Xue, K. L. Wang, Z. K. Wang, Y. Luo, D. Fenning, G. Xu, S. Nuryyeva, T. Huang, Y. Zhao, J. L. Yang, J. Zhu, M. Wang, S. Tan, I. Yavuz, K. N. Houk, Y. Yang, *Science* **2019**, *366*, 1509.
[27] J. V. Milić, N. Arora, M. I. Dar, S. M. Zakeeruddin, M. Grätzel, *Adv. Mater. Interfaces* **2018**, *5*, 1800416.
[28] E. A. Alharbi, A. Y. Alyamani, D. J. Kubicki, A. R. Uhl, B. J. Walder, A. Q. Alanazi, J. Luo, A. Burgos-Caminal, A. Albadri, H. Albrithen, M. H. Alotaibi, J. E. Moser, S. M. Zakeeruddin, F. Giordano, L. Emsley, M. Gratzel, *Nat. Commun.* **2019**, *10*, 3008.
[29] Y. Liu, S. Akin, L. Pan, R. Uchida, N. Arora, J. V. Milic, A. Hinderhofer, F. Schreiber, A. R. Uhl, S. M. Zakeeruddin, A. Hagfeldt, M. I. Dar, M. Gratzel, *Sci. Adv.* **2019**, *5*, 2543.
[30] D. Bi, C. Yi, J. Luo, J.-D. Décoppet, F. Zhang, S. M. Zakeeruddin, X. Li, A. Hagfeldt, M. Grätzel, *Nat. Energy* **2016**, *1*, 16142.
[31] S. Yang, S. Chen, E. Mosconi, Y. Fang, X. Xiao, C. Wang, Y. Zhou, Z. Yu, J. Zhao, Y. Gao, F. De Angelis, J. Huang, *Science* **2019**, *365*, 473.
[32] C. Xue, Z. Y. Yao, J. Zhang, W. L. Liu, J. L. Liu, X. M. Ren, *Chem. Commun. (Camb.)* **2018**, *54*, 4321.
[33] W. Q. Liao, Y. Zhang, C. L. Hu, J. G. Mao, H. Y. Ye, P. F. Li, S. D. Huang, R. G. Xiong, *Nat. Commun.* **2015**, *6*, 7338.
[34] A. Garcia-Fernandez, J. M. Bermudez-Garcia, S. Castro-Garcia, A. L. Llamas-Saiz, R. Artiaga, J. J. Lopez-Beceiro, M. Sanchez-Andujar, M. A. Senaris-Rodriguez, *Inorg. Chem.* **2018**, *57*, 3215.
[35] A. Garcia-Fernandez, J. M. Bermudez-Garcia, S. Castro-Garcia, A. L. Llamas-Saiz, R. Artiaga, J. Lopez-Beceiro, S. Hu, W. Ren, A. Stroppa, M. Sanchez-Andujar, M. A. Senaris-Rodriguez, *Inorg. Chem.* **2017**, *56*, 4918.
[36] W. F. Zhang, W. J. Pan, T. Xu, R. Y. Song, Y. Y. Zhao, C. Y. Yue, X. W. Lei, *Inorg. Chem.* **2020**, *59*, 14085.
[37] Z. Yuan, C. Zhou, Y. Tian, Y. Shu, J. Messier, J. C. Wang, L. J. van de Burgt, K. Kountouriotis, Y. Xin, E. Holt, K. Schanze, R. Clark, T. Siegrist, B. Ma, *Nat. Commun.* **2017**, *8*, 14051.
[38] Z. Wu, L. Li, C. Ji, G. Lin, S. Wang, Y. Shen, Z. Sun, S. Zhao, J. Luo, *Inorg. Chem.* **2017**, *56*, 8776.
[39] M. Shi, S.-S. Yu, H. Zhang, S.-X. Liu, H.-B. Duan, *J. Mol. Struct.* **2020**, *1206*, 127650.
[40] H.-B. Duan, S.-S. Yu, S.-X. Liu, H. Zhang, *RSC Adv.* **2017**, *7*, 23234.
[41] X. Song, G. Wei, J. Sun, C. Peng, J. Yin, X. Zhang, Y. Jiang, H. Fei, *Nat. Catal.* **2020**, *3*, 1027.
[42] Y.-J. She, S.-P. Zhao, Z.-F. Tian, X.-M. Ren, *Inorg. Chem. Commun.* **2014**, *46*, 29.
[43] H. Li, S. Yang, S. Gong, J. Wu, S. Pan, Z. Chen, Q. Zhao, C. Shou, Q. Shen, *J. Alloys Compd.* **2019**, *797*, 811.
[44] S. Jin, Y. Wei, B. Rong, Y. Fang, Y. Zhao, Q. Guo, Y. Huang, L. Fan, J. Wu, *J. Power Sources* **2020**, 450.
[45] I. Poli, S. Eslava, P. Cameron, *J. Mater. Chem. A* **2017**, *5*, 22325.
[46] Z. Xu, R. Chen, Y. Wu, R. He, J. Yin, W. Lin, B. Wu, J. Li, N. Zheng, *J. Mater. Chem. A* **2019**, *7*, 26849.
[47] P. Kour, M. Chenna Reddy, R. Naphade, S. Ogale, *APL Mater.* **2018**, 6.
[48] X. Liu, X. Wang, T. Zhang, Y. Miao, Z. Qin, Y. Chen, Y. Zhao, *Angew. Chem., Int. Ed. Engl.* **2021**, https://doi.org/10.1002/anie.202102538.
[49] D.-H. Kang, S.-Y. Kim, J.-W. Lee, N.-G. Park, *J. Mater. Chem. A* **2021**, *9*, 3441.
[50] T. Zhou, H. Lai, T. Liu, D. Lu, X. Wan, X. Zhang, Y. Liu, Y. Chen, *Adv. Mater.* **2019**, *31*, 1901242.
[51] Q. Jiang, L. Zhang, H. Wang, X. Yang, J. Meng, H. Liu, Z. Yin, J. Wu, X. Zhang, J. You, *Nat. Energy* **2016**, *2*, 16177.
[52] J. J. Yoo, S. Wieghold, M. C. Sponseller, M. R. Chua, S. N. Bertram, N. T. P. Hartono, J. S. Tresback, E. C. Hansen, J.-P. Correa-Baena, V. Bulović, T. Buonassisi, S. S. Shin, M. G. Bawendi, *Energy Environ. Sci.* **2019**, *12*, 2192.
[53] H. Wang, Z. Wang, Z. Yang, Y. Xu, Y. Ding, L. Tan, C. Yi, Z. Zhang, K. Meng, G. Chen, Y. Zhao, Y. Luo, X. Zhang, A. Hagfeldt, J. Luo, *Adv. Mater.* **2020**, *32*, 2000865.
[54] Y. Lin, Y. Bai, Y. Fang, Z. Chen, S. Yang, X. Zheng, S. Tang, Y. Liu, J. Zhao, J. Huang, *J. Phys. Chem. Lett.* **2018**, *9*, 654.
[55] Y. Zhang, P. Gao, E. Oveisi, Y. Lee, Q. Jeangros, G. Grancini, S. Paek, Y. Feng, M. K. Nazeeruddin, *J. Am. Chem. Soc.* **2016**, *138*, 14380.
[56] J. Liu, B. Chen, Q. Wang, R. Li, B. Shi, Y. Li, F. Hou, X. Cui, P. Wang, Y. Li, Y. Zhao, X. Zhang, *Appl. Phys. Lett.* **2019**, *115*, 233901.
[57] J. Zhuang, P. Mao, Y. Luan, X. Yi, Z. Tu, Y. Zhang, Y. Yi, Y. Wei, N. Chen, T. Lin, F. Wang, C. Li, J. Wang, *ACS Energy Lett.* **2019**, *4*, 2913.
[58] C. Xin, J. Zhang, X. Zhou, L. Ma, F. Hou, B. Shi, S. Pan, B. Chen, P. Wang, D. Zhang, X. Chen, Y. Zhao, A. A. Bakulin, Y. Li, X. Zhang, *ACS Appl. Energy Mater.* **2020**, *3*, 3318.
[59] X. Yang, Y. Fu, R. Su, Y. Zheng, Y. Zhang, W. Yang, M. Yu, P. Chen, Y. Wang, J. Wu, D. Luo, Y. Tu, L. Zhao, Q. Gong, R. Zhu, *Adv. Mater.* **2020**, *32*, 2002585.
[60] M. Hou, Y. Xu, B. Zhou, Y. Tian, Y. Wu, D. Zhang, G. Wang, B. Li, H. Ren, Y. Li, Q. Huang, Y. Ding, Y. Zhao, X. Zhang, G. Hou, *Adv. Funct. Mater.* **2020**, *30*, 2002366.
[61] P. Wang, R. Li, B. Chen, F. Hou, J. Zhang, Y. Zhao, X. Zhang, *Adv. Mater.* **2020**, *32*, 1905766.